J. Phys. D: Appl. Phys. 28 (1995) 1903–1918. Printed in the UK

Non-equilibrium coupled kinetics in stationary N_2–O_2 discharges

V Guerra and J Loureiro

Centro de Electrodinâmica da Universidade Técnica de Lisboa, Instituto Superior Técnico, 1096 Lisboa Codex, Portugal

Received 27 February 1995, in final form 23 May 1995

Abstract. A detailed study of the coupled electron and heavy-particle kinetics in a low-pressure stationary N_2–O_2 discharge is carried out. The model is based on the self-consistent solutions to the Boltzmann equation coupled to the rate balance equations for the vibrationally excited molecules $N_2(X\ ^1\Sigma_g^+, v)$ and $O_2(X\ ^3\Sigma_g^-, v')$, $NO(X\ ^2\Pi_r)$ molecules and $N(^4S)$ and $O(^3P)$ atoms. It is shown that the vibrational distribution of $N_2(X, v)$ plays a central role in the whole problem, affecting considerably the predicted concentrations of NO molecules and N atoms, whereas the concentration of O atoms is practically independent of both vibrational distributions. In particular, it is shown that, in the case of a rate coefficient of about 10^{-13} cm^3 s^{-1} for the reaction $N_2(X, v) + O \rightarrow NO + N$, the $N_2(X, v)$ molecules are strongly de-excited by vibrational–translational energy exchange processes associated with N_2–N collisions. In contrast, in the case of a higher value for this rate coefficient, the $N_2(X, v)$ molecules are efficiently destroyed by this mechanism. The contributions of the different processes to the total production of NO, N and O are evaluated and compared.

1. Introduction

Much interest has been devoted in the last few years to the study of DC and microwave discharges in N_2–O_2 mixtures, either experimentally [1–5] or theoretically [1, 2, 6]. Discharges in N_2–O_2 mixtures are studied with the purpose of material treatments or in order to test coating materials for space vehicles under conditions of atmospheric re-entry. On the other hand, discharges in O_2 with traces of N_2 are also studied due to the broadening use of oxygen plasma technology in many applications, such as etching and surface treatments of polymers [7, 8] or silicon oxidation [9]. Furthermore, N_2–O_2 plasmas are also studied for the synthesis of nitric oxides [10–12] or within the framework of studies in non-equilibrium plasmochemical systems in general.

At the same time, much effort has been concentrated for the purpose of gaining a deeper understanding of the fundamental physics of the non-equilibrium kinetics in molecular systems. Great impetus to this research field has come from the determination of accurate sets of electron cross sections from swarm experiments for many molecular gases, as well as from a good knowledge of the rate coefficients for many molecular reactions. This fact has allowed the development of theoretical models for DC and microwave discharges in pure N_2 [13–16] and pure O_2 [17–20].

However, when we deal with mixtures of molecular gases the situation becomes more and more complex due to the interplay of the different microscopic processes acting in the medium. The solution of the resulting complex kinetic problem requires a joint contribution from different data. Unfortunately, in most cases accurate knowledge of the electron cross sections and rate coefficients for the different microscopic processes does not exist and some data need to be estimated.

In spite of the lack of data, it has been possible to develop theoretical models in order to interpret various experiments conducted on DC discharges, either in pure N_2 [14] or in pure O_2 [18], or in mixtures of the two gases [2, 6]. In the latter case, it was possible in [6] to obtain excellent agreement between theoretical predictions and experiment, using a critical choice of data from the literature and deriving unknown data from a best fit of calculated concentrations of different molecular and atomic species present in the discharge to the measured ones. In particular, good agreement for the concentrations of $NO(X\ ^2\Pi_r)$ molecules and $O(^3P)$ atoms has been obtained by fitting the rate coefficient for the main reaction leading to the formation of NO and the probabilities of re-association on the wall of N and O atoms.

Here, we propose a different approach. The aim of this paper is to give an insight into the effects of the predicted rate coefficients for some specific processes on the discharge kinetics. In particular, we will show that the uncertainties in the rate coefficients for the de-activation of $N_2(X\ ^1\Sigma_g^+, v > 0)$ vibrationally excited molecules through vibrational–translational (V–T) energy exchanges in collisions with N or O atoms may considerably affect the calculated concentrations of N atoms and NO molecules,

0022-3727/95/091903+16$19.50

Table 1. Kinetics of $N_2(X, v)$ molecules, with $0 \leq v \leq 45$.

e–V	$e + N_2(X, v) \rightleftharpoons e + N_2(X, w)$	(R1)
V–V N_2–N_2	$N_2(X, v) + N_2(X, w) \rightleftharpoons N_2(X, v-1) + N_2(X, w+1)$	(R2)
V–T N_2–N_2	$N_2(X, v) + N_2 \rightleftharpoons N_2(X, v-1) + N_2$	(R3)
V–V N_2–O_2	$N_2(X, v) + O_2(X, v') \rightleftharpoons N_2(X, v-1) + O_2(X, v'+1)$	(R4)
V–T N_2–O_2	$N_2(X, v) + O_2 \rightleftharpoons N_2(X, v-1) + O_2$	(R5)
V–T N_2–N	$N_2(X, v) + N \rightleftharpoons N_2(X, w < v) + N$	(R6)
	$N_2(X, v) + N \rightleftharpoons N + N_2(X, w < v)$	(R7)
V–T N_2–O	$N_2(X, v) + O \rightleftharpoons N_2(X, v-1) + O$	(R8)
W	$N_2(X, v) + \text{wall} \rightarrow N_2(X, v-1)$	(R9)
e–D:	$e + N_2(X, v) \rightarrow e + N + N$	(R10)
V–D	$N_2(X, v) + N_2(X, v = 45) \rightarrow N_2(X, v-1) + N + N$	(R11)
	$O_2(X, v') + N_2(X, v = 45) \rightarrow O_2(X, v'-1) + N + N$	(R12)
	$M + N_2(X, v = 45) \rightarrow M + N + N \qquad M = N_2, O_2 \text{ or } O$	(R13)
R	$N + N \rightarrow N_2(X, v = 0)$	(R14)
NO	$N_2(X, v) + O \rightarrow NO + N$	(R15)
	$NO + N \rightarrow N_2(X, v) + O$	(R16)

respectively. We note that the V–T exchanges in N_2–N collisions have been neglected in [6]. However, the effects of these V–T processes become progressively smaller with the increase of the rate coefficient for the reaction $N_2(X, v) + O \rightarrow NO + N$, which is the predominant mechanism for the formation of NO and N in N_2–O_2 glow discharges. Owing to the present state of knowledge of the basic data for various microscopic processes, the point of view presented in this paper is essential in order to investigate in detail such complex systems.

For this purpose, we present a self-consistent and stationary analysis based on solutions to the coupled system formed by the electron Boltzmann equation, the two systems of rate balance equations for the populations in the vibrational levels $N_2(X\ ^1\Sigma_g^+, v)$ and $O_2(X\ ^3\Sigma_g^-, v')$, and the rate balance equations for the concentrations of $N(^4S)$, $O(^3P)$ and $NO(X\ ^2\Pi_r)$ species. From the present model, we obtain the electron energy distribution function, the *vibrational distributions of both ground-state molecules and* the concentrations of N and O atoms and NO molecules. Calculations of other relevant quantities are carried out and their dependences on the rate coefficients of specific processes are discussed.

In section 2 we present in detail the theoretical model used in this paper, emphasizing the various assumptions used. In section 3 we summarize the data used in the calculations and we discuss the reasons for the present choice. The results of the model are presented and discussed in section 4. Finally, section 5 summarizes the main conclusions.

2. The kinetic model

The present analysis is based on the simultaneous, steady-state solutions to the homogeneous electron Boltzmann equation, the two systems of rate balance equations for the vibrational populations $N_2(X\ ^1\Sigma_g^+, 0 \leq v \leq 45)$ and $O_2(X\ ^3\Sigma_g^-, 0 \leq v' \leq 15)$, and the rate balance equations for the atomic species $N(^4S)$ and $O(^3P)$ and the ground-state molecule $NO(X\ ^2\Pi_r)$. Owing to the non-negligible populations in the vibrationally excited levels, the Boltzmann equation is coupled to the systems for the vibrational populations through both inelastic and superelastic electronic–vibrational (e–V) collisions. The equations for the other heavy species present in the discharge are strongly coupled to one another and to the equations for the vibrational levels.

2.1. Electron and vibrational kinetics

The steady-state, homogeneous electron Boltzmann equation is solved under the classical two-term expansion in spherical harmonics, which is valid assuming small anisotropies from the electric field. This has been a standard approach since the sixties [21]. The final form taken by this equation for the case of a mixture of two molecular gases can be found in [22]. Here, the Boltzmann equation is solved taking into account collisions of all types (elastic, excitation and de-excitation of rotational levels, excitation and de-excitation of vibrational levels, excitation of electronic states and ionization) both for N_2 and for O_2, as well as electron collisions with the dissociated N and O species. Excitation and de-excitation of rotational levels have been treated here in the continuous approximation discussed in [21], using, for N_2 and O_2 respectively, the rotational energy constants 2.5×10^{-4} eV [23] and 1.8×10^{-4} eV [24], and the electric quadrupole moments 1.01 [21] and 0.29 [25] in units of ea_0^2 (e and a_0 are the absolute value of the electron charge and the Bohr radius, respectively). The peak in the electron cross sections for rotational excitation of N_2 at 2.3 eV, attributed to a $N_2^-(^2\Pi_g)$ shape resonance [26], has been included with the cross sections for vibrational excitation. Inelastic and superelastic collisions of electrons with vibrationally excited molecules $N_2(X, v > 0)$ and $O_2(X, v' > 0)$ have been taken into account, while the excitation of electronic states was treated as a single energy-loss process assuming, in this case, that all the molecules are in the ground vibrational level, $N_2(X, v = 0)$ or $O_2(X, v' = 0)$. Furthermore, superelastic collisions of electrons with molecules in electronically excited states have been neglected. Finally, the ionization process has been treated similarly to an excitation with a single energy loss and the creation of secondary electrons was neglected.

The numerical procedure used for solving the Boltzmann equation is exactly the same as in previous papers [13] and in basic trends it consists of converting the Boltzmann equation into a set of coupled algebraic equations by finite-differencing the electron energy axis.

This approach to the Boltzmann equation allows us to obtain the electron energy distribution function (EEDF) as a function of the following set of independent parameters: the ratio of the electric field to the total gas number density, E/N; the vibrational temperatures of the electronic ground state for both gases, $T_v(N_2)$ and $T_v(O_2)$; the gas temperature, T_g; and the fractional composition of the mixture, $[O_2]/N$, $[N]/N$, $[O]/N$ and $[NO]/N$, with $N = [N_2] + [O_2] + [N] + [O] + [NO]$. Our analysis shows that, under the present conditions, the dependence of the EEDF on the parameters $T_v(O_2)$, T_g, $[N]/N$, $[O]/N$ and $[NO]/N$ has only a minor influence.

The Boltzmann equation is therefore coupled through the fractional vibrational populations $\delta_v = [N_2(X, v)]/[N_2]$ and $\delta_{v'} = [O_2(X, v')]/[O_2]$, that is through the vibrational distribution functions (VDFs) for both gases, to the systems of steady-state rate balance equations for these populations. The degree of excitation of each VDF is characterized by the vibrational temperatures $T_v(N_2)$ and $T_v(O_2)$. Omitting negligible processes, the equations for a given vth or v'th level, in N_2 or in O_2, can be written in a symbolic form as follows:

$$\left(\frac{dN_v}{dt}\right)_{e-V} + \left(\frac{dN_v}{dt}\right)_{V-V}^{N_2-N_2} + \left(\frac{dN_v}{dt}\right)_{V-T}^{N_2-N_2} + \left(\frac{dN_v}{dt}\right)_{V-V}^{N_2-O_2} + \left(\frac{dN_v}{dt}\right)_{V-T}^{N_2-O_2} + \left(\frac{dN_v}{dt}\right)_{V-T}^{N_2-N} + \left(\frac{dN_v}{dt}\right)_{V-T}^{N_2-O} + \left(\frac{dN_v}{dt}\right)_{W} + \left(\frac{dN_v}{dt}\right)_{eD} + \left(\frac{dN_v}{dt}\right)_{VD} + \left(\frac{dN_v}{dt}\right)_{R} + \left(\frac{dN_v}{dt}\right)_{NO} = 0 \quad (1)$$

$$\left(\frac{dN_{v'}}{dt}\right)_{e-V} + \left(\frac{dN_{v'}}{dt}\right)_{V-V}^{O_2-O_2} + \left(\frac{dN_{v'}}{dt}\right)_{V-T}^{O_2-O_2} + \left(\frac{dN_{v'}}{dt}\right)_{V-V}^{O_2-N_2} + \left(\frac{dN_{v'}}{dt}\right)_{V-T}^{O_2-N_2} + \left(\frac{dN_{v'}}{dt}\right)_{V-T}^{O_2-O} = 0. \quad (2)$$

The various terms in equations (1) and (2) account for a large number of processes listed in tables 1 and 2. The e–V, V–V and V–T processes denote the mechanisms of electronic–vibrational, vibrational–vibrational, and vibrational–translational energy exchanges, respectively, including collisions between equal and different collision partners, N_2–N_2, O_2–O_2, N_2–O_2, N_2–N, N_2–O and O_2–O. The V–T reactions in N_2–N collisions include both a direct process (R6) and a reactive one (R7), in which atomic exchange occurs between the two collision partners [27–29]. For the V–V and V–T reactions we consider only single-quantum transitions, which are the most likely ones, except for V–T reactions in the system N_2–N. The reaction (R9) takes into account the de-activation of vibrationally excited molecules $N_2(X, v)$ through collisions on the wall. For this process also, only single-quantum transitions are considered. The reactions (R11)–(R13) take into account dissociation by the V– V and V–T processes in N_2, which is modelled as a transition from the last bound level $v = 45$ to a pseudo-level in the continuum [30].

Thus, the total dissociation rate of N_2 (in $cm^{-3}\ s^{-1}$) is, according to reactions (R10)–(R13), given by

$$v_{diss} = n_e \sum_{v=0}^{45} [N_2(X, v)] C_{diss}^e + [N_2(X, 45)] \times \left(\sum_{v=1}^{45} [N_2(X, v)] P_{45,46}^{v,v-1} + [N_2] P_{45,46}^{N_2-N_2} + \sum_{v'=1}^{15} [O_2(X, v')] P_{45,46}^{v',v'-1} + [O_2] P_{45,46}^{N_2-O_2} + [O] P_{45,46}^{N_2-O} \right). \quad (3)$$

The first term on the right-hand side of equation (3) accounts for dissociation by electron impact (R10), n_e and C_{diss}^e denoting the electron number density and the electron dissociation rate coefficient, respectively. Although in the present model we have considered collisions of electrons with N_2 molecules in different individual vth levels up to $v = 45$, due to the lack of reliable data the electron dissociation rate coefficient has been considered equal for all levels. The reactions (R15) and (R16) result in formation and destruction of NO molecules, both having a non-negligible influence on the VDF of N_2 (see discussion in section 4). Finally, reaction (R14) takes into account, in a symbolic form, the process of atomic re-association in N_2. Here, we just assume that, under steady-state conditions, the total number of $N_2(X, v)$ molecules must be constant:

$$\sum_{v=0}^{45} [N_2(X, v)] = [N_2] = \text{constant}. \quad (4)$$

Therefore, the total atomic re-association rate must exactly compensate for the dissociation rate given by equation (3) plus the rates for all other processes destroying $N_2(X, v)$ molecules:

$$v_{reass} = v_{diss} + [O]\left(\sum_{v=13}^{45} [N_2(X, v)] K_{15}^v \right) - [NO][N] \times \left(\sum_{v=1}^{5} K_{16}^v \right) \quad (5)$$

where K_{15}^v and K_{16}^v denote the rate coefficients of reactions (R15) and (R16), respectively. Due to the lack of information about atomic re-association, we assume that it populates the vibrational level $v = 0$ only. In a previous work [13] the effects of atomic re-association into other vth levels have been analysed in detail for N_2.

Owing to the large magnitude of the V–T rates for O_2–O collisions and the relatively small electron rate coefficients for vibrational excitation of O_2 as compared to those for N_2, the VDF of O_2 is poorly excited, except in the case of a discharge in N_2 with a small admixture of

Table 2. Kinetics of $O_2(X, v')$ molecules, with $0 \leq v' \leq 15$.

e–V	$e + O_2(X, v') \rightleftharpoons e + O_2(X, w')$	(R17)
V–V O_2–O_2	$O_2(X, v') + O_2(X, w') \rightleftharpoons O_2(X, v' - 1) + O_2(X, w' + 1)$	(R18)
V–T O_2–O_2	$O_2(X, v') + O_2 \rightleftharpoons O_2(X, v' - 1) + O_2$	(R19)
V–V O_2–N_2	$O_2(X, v') + N_2(X, v) \rightleftharpoons O_2(X, v' - 1) + N_2(X, v + 1)$	(R20)
V–T O_2–N_2	$O_2(X, v') + N_2 \rightleftharpoons O_2(X, v' - 1) + N_2$	(R21)
V–T O_2–O	$O_2(X, v') + O \rightleftharpoons O_2(X, v' - 1) + O$	(R22)

Table 3. Kinetics of $NO(X^2\Pi_r)$ molecules.

Reaction R15		
$N + O_2 \rightarrow NO + O$		(R23)
$N_2(A\,^3\Sigma_u^+) + O \rightarrow NO + N^*$		(R24)
$N + O + N_2 \rightarrow NO + N_2$		(R25)
Reaction R16		
$O + NO + M \rightarrow NO_2 + M$	$M = N_2$ or O_2	(R26)

Table 4. Kinetics of $N(^4S)$ atoms.

Reaction R10	
Reactions (R11)–(R13)	
Reaction (R15)	
$N + \text{wall} \rightarrow \frac{1}{2}N_2$	(R27)
$N + N + N_2 \rightarrow N_2^* + N_2$	(R28)
$N + N_2(A\,^3\Sigma_u^+) \rightarrow N^* + N_2$	(R29)
$e + N \rightarrow e + N^*$	(R30)
Reactions (R16), (R23) and (R25)	

Table 5. Kinetics of $O(^3P)$ atoms.

$e + O_2(X, v') \rightarrow e + O + O$	(R31)
$N_2(B\,^3\Pi_g) + O_2 \rightarrow N_2 + O + O$	(R32)
Reactions (R16) and (R23)	
$O + \text{wall} \rightarrow \frac{1}{2}O_2$	(R33)
Reactions (R15), (R24)–(R26)	

O_2 (see discussion in section 4). Thus, mechanisms for O_2 other than those listed in table 2 have no marked influence on the VDF for that gas. Finally, we note that, due to the relatively small concentration of NO and to the larger mass of this molecule as compared to those of the atomic species N and O, the vibrational relaxation of N_2 and O_2 in collisions with NO has been neglected in equations (1) and (2). Furthermore, the vibrational kinetics of NO does not play any significant role, so that we have discarded in the model the vibrational distribution of these molecules.

2.2. Kinetics of NO, N and O species

The electron and the vibrational kinetics of $N_2(X, v)$ and $O_2(X, v')$ molecules are strongly coupled to the various reactions for formation and destruction of $NO(X\ ^2\Pi_r)$ molecules and ground-state atoms $N(^4S)$ and $O(^3P)$ listed in tables 3, 4 and 5, respectively. Furthermore, some of these reactions play a role in more than one of the kinetics (such as reactions R15 and R16). A detailed analysis of each of these processes will be conducted in section 3, together with a discussion of the different data. Here, we simply note that some of the reaction products are indicated by the symbols N_2^* or N^*, which denote, in the present model, unspecified electronically excited states.

2.3. Proper variables

As stated before, the Boltzmann equation is solved self-consistently with the vibrational rate balance equations (1) and (2) and the rate balance equations for NO molecules and N and O atoms. This set of equations yields the EEDF, $f(u)$ (normalized here such that $\int_0^\infty f(u)\sqrt{u}\,du = 1$, where $u = \frac{1}{2}mv^2$ denotes the electron energy), the VDFs, $\delta_v = [N_2(X, v)]/[N_2]$ and $\delta_{v'} = [O_2(X, v')]/[O_2]$, and the fractional concentrations $\delta(NO) = [NO]/N$, $\delta(N) = [N]/N$ and $\delta(O) = [O]/N$. The degrees of vibrational excitation of the two molecules are characterized by the temperatures $T_v(N_2)$ and $T_v(O_2)$.

Under the present formulation, the results are obtained as a function of the independent parameters E/N (or E/p, where p denotes the total gas pressure), degree of ionization n_e/N, fractional concentration of N_2 in the mixture $\delta(N_2)$, total gas density N (or pressure p), gas temperature T_g and discharge tube radius R. However, due to the numerical procedure used to solve these equations, it is useful to use $T_v(N_2)$ as an independent parameter instead of n_e/N. It is worth noting at this point that the inclusion of the heterogeneous reactions (R9), (R27) and (R33) means that the product NR needs to be given as an input parameter in the present model. Furthermore, the inclusion of the three-body processes (R25), (R26) and (R28) means that the variables N and R need to be given separately. As a consequence of this the electron density, n_e, and the discharge current, I, are also determined by the present model.

Obviously, in a fully self-consistent model for a N_2–O_2 discharge, once E/N is given the total gas density N is no longer an independent parameter. The two parameters are linked through the requirement that, under steady-state conditions, the production of new electrons (by electron impact or by collisions between heavy particles) proceeds at a rate that compensates exactly for the rate of electron loss (by ambipolar diffusion or free fall to the wall). It is well known that this requirement determines the reduced sustaining field E/N necessary for the steady-state operation of the discharge as a function of N, the discharge current I, and $\delta(N_2)$, for a given value of R, provided that T_g is determined self-consistently. However, the determination of the discharge characteristics is outside the scope of the present paper.

Table 6. Inelastic and super-elastic processes in the electron Boltzmann equation.

Nitrogen
$e + N_2(X, v) \rightleftharpoons e + N_2(X, w)$
$(v = 0, \ldots, 9; w = v + 1, \ldots, 10)$
$e + N_2(X, v = 0) \rightarrow e + N_2(Y)$
$(Y = A\ ^3\Sigma_u^+, B\ ^3\Pi_g, W\ ^3\Delta_u, B'\ ^3\Sigma_u^-, a'\ ^1\Sigma_u^-,$
$a\ ^1\Pi_g, w\ ^1\Delta_u, C\ ^3\Pi_u, E\ ^3\Sigma_g^+, a''\ ^1\Sigma_g^+, c'\ ^1\Sigma_u^+, c\ ^1\Pi_u,$
$b\ ^1\Pi_u, b'\ ^1\Sigma_u^+)$
$e + N_2(X, v = 0) \rightarrow e + N_2^+ + e$
$e + N(^4S) \rightarrow e + N(Y)$
$(Y = {}^2D, {}^2P)$
Oxygen
$e + O_2(X, v') \rightleftharpoons e + O_2(X, w')$
$(v' = 0, \ldots, 3; w' = v' + 1, \ldots, 4)$
$e + O_2(X, v' = 0) \rightarrow e + O_2(Y)$
$(Y = a\ ^1\Delta_g, b\ ^1\Sigma_g^+,$ states with energy losses at
4.5, 6.0, 8.4, 9.97 and 14.7 eV)
$e + O_2(X, v' = 0) \rightarrow e + O_2^+ + e$
$e + O(^3P) \rightarrow e + O(Y)$
$(Y = {}^1D, {}^1S, {}^3S)$

3. Collisional data

3.1. Electron cross sections

The electron cross sections used in this paper to solve the Boltzmann equation are the same as in previous works in pure N_2 [13] and pure O_2 [18], so the reader should refer to these papers for details. The only exception concerns collisions of electrons with ground-state atoms $N(^4S)$ which have been discarded in [13]. The cross sections for such processes have been taken from [31], insofar as they concern the momentum transfer cross section, and from [32] for the excitation of the $N(^2D)$ and $N(^2P)$ states. We note that the excitations of electronic states of N_2 and O_2 were treated as single energy-loss processes, because in a previous paper [33] we have shown that the inclusion of individual transitions between vibrational levels in N_2 introduces only minor modifications in the EEDF. Finally, the collisions of electrons with NO molecules also produce only negligibly small modifications, so that they have been discarded. Table 6 shows a list of the various inelastic and superelastic processes included in the Boltzmann equation.

For dissociation of N_2 by electron impact, we have used the total cross section proposed in [34], which relies on the assumption that the predissociation of the numerous $^1\Pi_u$ and $^1\Sigma_u^+$ valence and Rydberg states of N_2, with energy thresholds larger than 11 eV, is the dominant mechanism for dissociation. Other states of N_2, such as the $a\ ^1\Pi_g$ state and the triplet $B\ ^3\Pi_g$ and $C\ ^3\Pi_u$ states, in higher vibrational levels, also contribute to pre-dissociation. The total dissociation cross section so obtained is in very good agreement with other measurements [35]. In what concerns the dissociation of O_2, the reactions referred to in table 6 as the 6.0 and 8.4 eV energy-loss processes correspond to two different channels for dissociation, leading to the creation of two $O(^3P)$ atoms and to a pair of $O(^3P)$ and $O(^1D)$ atoms, respectively. As in the present model we only consider ground-state atoms, therefore discarding the kinetics of excited atomic species, we assume that both reactions give two $O(^3P)$ atoms.

3.2. V–V and V–T rates

All the calculations in section 4 were performed for $T_g = 500$ K, which represents a typical average value for the operating conditions of a low-pressure N_2–O_2 glow discharge. Therefore, the data for V–V and V–T rates have been chosen from the literature or calculated for this specific temperature.

The V–V and V–T rate coefficients for N_2–N_2 collisions (given by reactions (R2) and (R3) in table 1) have been obtained by fitting a SSH (Schwartz, Slawsky and Herzfeld) scaling law [36, 37], as modified in [38, 39], to the results obtained by Billing and co-workers [40, 41] using a three-dimensional collision model which includes an intermolecular potential with both long- and short-range interactions. It is worthy of note at this point that the SSH theory ignores the attractive part of the potential. Nevertheless, although a large number of publications on the subject have appeared in recent years using more accurate collision models [42, 43], the number of transitions for which the calculations have been performed is limited. Here, in order to obtain the V–V and V–T probabilities for all the transitions, we have fitted scaling laws of SSH type to the actual rates of Billing [40, 41].

The V–V rate coefficient for the transition $(1, 0) \rightarrow (0, 1)$ in N_2–O_2 collisions has been obtained by shock interferometry and infrared emission as reported in the compilation [44]. However, this coefficient has been measured for $T_g \geq 800$ K only, so that here we have integrated the transition probabilities calculated in [45] over a Maxwellian distribution for the relative velocity of the molecules. The coefficient obtained using this procedure is close to that presented in [44] for $T_g = 800$ K. For the other V–V transitions indicated in (R4), we have used SSH scaling laws with a length characterizing the short range exponential of the intermolecular potential $L = 0.3$ Å (for the same reasons as in [22]), subject to the condition that, in the case of the nearly resonant transition

$$N_2(X, v = 28) + O_2(X, v' = 0) \rightleftharpoons N_2(X, v = 27) + O_2(X, v' = 1) \quad (6)$$

the corresponding rate coefficient should, according to the SSH theory, be close to $28P_{1,0}^{0,1}(O_2\text{–}O_2)$, where $P_{1,0}^{0,1}(O_2\text{–}O_2)$ denotes the rate coefficient for the transition $(1, 0) \rightarrow (0, 1)$ associated with O_2–O_2 collisions given in [46]. Note that we have not simply used the expressions from the SSH theory [22], because it is known that this theory overestimates the actual rates [40]. In the present calculations, the energies of the vibrational levels of N_2 and O_2 are given by $E_v = \hbar\omega[(v+0.5) - \chi_e(v+0.5)^2]$, with the anharmonic Morse oscillator parameters $\omega(N_2) = 4.44 \times 10^{14}\ s^{-1}$, $\omega(O_2) = 2.98 \times 10^{14}\ s^{-1}$, $\chi_e(N_2) = 6.073 \times 10^{-3}$ and $\chi_e(O_2) = 7.581 \times 10^{-3}$ [47]. The coefficients for the reverse reactions are obtained by detailed balancing.

In what concerns the V–T exchanges in N_2–O_2 collisions, given by reaction (R5), no data are available, excepting those calculated in [48] and only for a few

transitions. So, here we scaled these coefficients from those for the V–T N_2–N_2 transitions using, once again, the SSH theory. The ratio between the coefficients for the vibrational de-excitation of a given vth level through both processes is, in the case of the adiabatic limit [36–39], given by

$$\frac{P_{v,v-1}^{N_2-O_2}}{P_{v,v-1}^{N_2-N_2}} = \frac{P_{1,0}^{N_2-O_2}}{P_{1,0}^{N_2-N_2}} \exp[(\delta_{VT(N_2-O_2)} - \delta_{VT(N_2-N_2)})(v-1)] \tag{7}$$

with

$$\frac{P_{1,0}^{N_2-O_2}}{P_{1,0}^{N_2-N_2}} = \left(\frac{\mu_{(N_2-O_2)}}{\mu_{(N_2-N_2)}}\right)^{1/2} \left(\frac{d_{(N_2-O_2)}}{d_{(N_2-N_2)}}\right)^2 \frac{F(Y_{1,0}^{N_2-O_2})}{F(Y_{1,0}^{N_2-N_2})} \tag{8}$$

and where $\delta_{VT(N_2-N_2)}$ and $\delta_{VT(N_2-O_2)}$ are given by the expression

$$\delta_{VT} = 4\chi_e(N_2)(\hbar\omega(N_2))^{2/3} \left(\frac{\pi L}{\hbar}\right)^{2/3} \left(\frac{\mu}{2KT_g}\right)^{1/3} \tag{9}$$

using the corresponding value of the reduced collisional mass μ in N_2–N_2 and N_2–O_2 collisions. The intermolecular length has been taken as $L = 0.3$ Å in the N_2–O_2 system (that is, using the same value as for the V–V exchanges) and by matching a law of SSH type with expression (9) to the rate coefficients for V–T N_2–N_2 collisions. Furthermore, d and $F(Y_{1,0})$ denote the distance of closest approach and the adiabaticity factor in the SSH theory (see equation (18) in [22]).

So far, only single-quantum transitions have been considered, since they are the most likely ones. The exception is related to the V–T exchanges in N_2–N collisions where the effect of multi-quantum transitions is known to be important. Furthermore, we consider two different reactions according to [27–29]. A direct process (R6) and a reactive one, given by (R7) in table 1, in which atomic exchange occurs between the collision partners. The corresponding rate coefficients have been calculated in [27–29] for a large number of transitions. Here, we have fitted these results in order to obtain a complete set, which was further subjected to the following restrictions: $P_{v,w}^{N_2-N} = 0$ for $|v-w| > 5$; $P_{v,w}^{N_2-N}$ independent of the wth level and given by the same expression for all the transitions with the same vth level, with from one to five quanta.

For the V–T N_2–O collisions, we have used, in the case of the vibrational de-excitation of the level $v = 1$, the fitting presented in [1] to the results reported in [49, 50]; for the other transitions (R8) we have simply scaled the rate coefficients using a linear dependence on the vth quantum number: $P_{v,v-1} = vP_{1,0}$. Note that, using this expression, we are assuming $\delta_{VT} = 0$ in the expression derived from the SSH theory:

$$P_{v,v-1} = P_{1,0}v\exp[\delta_{VT}(v-1)]. \tag{10}$$

It is still worth noting here that, due to the relatively high magnitude reported for the rate coefficient $P_{1,0}$, we would have obtained extremely high rate coefficients $P_{v,v-1}$ for the higher vth levels, had we used a non-zero value for δ_{VT}.

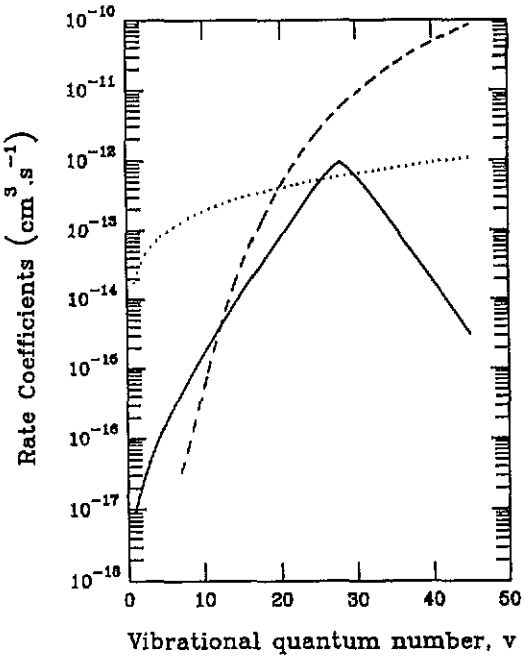

Figure 1. Rate coefficients for the V–V energy exchanges $N_2(v) + O_2(v'=0) \rightarrow N_2(v-1) + O_2(v'=1)$ (full curve) and for the V–T exchanges in N_2–N collisions (broken curve) and in N_2–O collisions (dotted curve), as a function of the vth quantum number in N_2 and for $T_g = 500$ K. The broken curve represents the sum $\sum_{w=0}^{v-1} P_{v,w}^{N_2-N}$ (see text).

The relative magnitudes of the rate coefficients for some of these processes can be evaluated from figure 1. As a function of the vth level in N_2, we plot (i) the rate coefficients for the V–V exchanges in N_2–O_2 collisions associated with the transitions $(v, v'=0) \rightarrow (v-1, v'=1)$ (full curves); (ii) the sum on the wth level of the rate coefficients for both types of V–T exchanges ((R6) and (R7)) in N_2–N collisions, $\sum_{w=0}^{v-1} P_{v,w}^{N_2-N}$ (broken curve), with $P_{v,w}^{N_2-N} = 0$ for $w < (v-5)$; and (iii) the rate coefficients for the V–T exchanges in N_2–O collisions (dotted curve). The maximum on the full curve corresponds to the nearly resonant transition (6).

Let us consider now the rate coefficients for equation (2). The rate coefficients for the V–V energy exchanges in O_2–O_2 collisions (R18) associated with the transitions $(1, v') \rightarrow (0, v'+1)$ have been taken from [46]. The coefficients for other transitions were obtained using a SSH scaling law with $L = 0.17$ Å [51].

The rate coefficients for the V–T exchanges in O_2–O_2 collisions (R19) have been taken from [46] as well, using the SSH theory with $L = 0.17$ Å to obtain the lacking coefficients. The value for $P_{1,0}$ so obtained, for the gas temperature $T_g = 500$ K, is larger by a factor of two than that obtained by extrapolation of the measurements reported in [52] to low temperatures . It should be pointed out, however, that the extrapolation to lower temperatures of experimental data underestimates the actual rates [53, 54].

The rate coefficients for the V–T transitions in O_2-N_2 collisions (R21) have been obtained using a similar procedure to that described for the case of reaction (R5), but here we scale the rate coefficients from those for the V–T O_2–O_2 transitions with $L = 0.3$ Å.

Finally, the rate coefficient for the V–T $1 \rightarrow 0$ exchange in O_2–O collisions (R22) has been taken from [55]. For $T_g = 500$ K this value is in good agreement with the result presented in [56] and is about two times larger than those measured in [57] and calculated in [58]. For the other transitions, we have used the scaling law $P_{v',v'-1} = v'P_{1,0}$, that is $\delta_{VT} = 0$ in equation (10), due to the same reasons as discussed before for reaction (R8). Still due to similar reasons, we have preferred to use this scaling law instead of that proposed in [59]: $P_{v',v'-1} = (3v' - 2)P_{1,0}$.

3.3. Rate coefficients of other reactions and wall processes

Reactions (R15) and (R16) in table 1, involving the destruction and the formation of vibrationally excited $N_2(X, v)$ molecules, also play an important role in the kinetics of NO(X) molecules and $N(^4S)$ and $O(^3P)$ atoms. Thus, the destruction of $N_2(X, v)$ molecules can occur through reaction (R15), which is the main source of NO molecules. Reaction (R15) was investigated in the context of the kinetics in the upper atmosphere [60] and within the studies of non-equilibrium plasmochemical synthesis of nitric oxides [10–12]. Unfortunately, there are no measurements of the rate coefficient for this reaction, K_{15}^v, and the calculations are in serious disagreement, by two orders of magnitude [61–63]. All calculations agree in considering a very sharp increase of the rate coefficient with the vth quantum number up to $v = 13$, and a small dependence for $v \geq 13$. Here, we use $K_{15}^v = 0$ for $v < 13$ and $K_{15}^v = 10^{-13}$ cm^3 s^{-1} for $v \geq 13$, which corresponds to an average value among those reported in the literature. However, we must note that a recent model developed in our laboratory [6] has shown that this coefficient might be larger than the majority of the previous determinations. In [6] had been found the value 10^{-11} cm^3 s^{-1} from a best agreement with the relative variation of the $N_2^+(B)$ 391.4 nm band, in a N_2–O_2 discharge at $p = 2$ Torr. Nevertheless, we have preferred here to keep the above-mentioned average value for the purposes of the present discussion as the previous estimation may be affected by the neglect of the V–T exchanges in N_2–N collisions. In section 4 we will discuss the changes caused in the results by considering other values for K_{15}^v.

The reverse of (R15) is reaction (R16) which results in excitation of the levels $v = 0$–12. The percentage of the energy transferred to the vibrational mode in reaction (R16) is about 25% [64], which corresponds on the average to the excitation of three vibrational quanta of N_2. Here, we assume that, due to the very fast V–V energy exchanges in N_2–N_2 collisions, some of this energy is transferred to near-lying levels. Thus, we arbitrarily assume that 40% of the energy remains in the level $v = 3$, 40% is equally transferred to the levels $v = 2$ and $v = 4$, and 20% goes into the levels $v = 1$ and $v = 5$. The total rate coefficient for reaction (R16), $K_{16} = 1.05 \times 10^{-12} T_g^{1/2}$ cm^3 s^{-1}, with T_g in K, has been taken from [65].

The other most important reactions determining the populations of NO(X) molecules are listed in table 3. Reaction (R23) is an important mechanism for NO production and N losses in mixtures predominantly formed by O_2 and for the lower values of $T_v(N_2)$ ($\lesssim 3500$ K). Here, we use for this reaction the rate proposed in [66] (see also [65]), $K_{23} = 1.1 \times 10^{-14} T_g \exp(-3150/T_g)$ cm^3 s^{-1}. Other more recent works [67, 68] have reasonably confirmed this result. For the reaction (R24) we have used the rate coefficient $K_{24} = 7 \times 10^{-12}$ cm^3 s^{-1} according to the discussion in [69, 70]. The atomic excited species N* formed by reaction (R24) is, in the present case, the metastable species $N(^2D)$ only. However, the kinetics of the N* species are not included in our model. For the three-body reaction (R25) we have used the value proposed in [65], $K_{25} = 1.76 \times 10^{-31} T_g^{-1/2}$ cm^6 s^{-1}, which corresponds to one of the largest values reported in the literature (see also [44]). We note, however, that reaction (R25) always has a vanishingly small effect in determining the populations of NO molecules. Finally, for reaction (R26) we have used the expressions proposed in [65].

For the other reactions involved in the kinetics of $N(^4S)$ atoms (see table 4), we have used the rate coefficient $K_{28} = 8.27 \times 10^{-34} \exp(500/T_g)$ cm^{6}s^{-1} [65] for the three-body reaction (R28), which is in reasonable agreement with that proposed in [71]. For reaction (R29) we have used the value $K_{29} = 4 \times 10^{-11}$ cm^3 s^{-1} [72], close to the value 5×10^{-11} cm^3 s^{-1} proposed in [73], where N* in table 4 denotes an $N(^2D)$ or $N(^2P)$ atom. The electron rate coefficients of reaction (R30), with N* = $N(^2D)$ or $N(^2P)$, have been calculated in this work using the electron cross sections given in [32] (see also [14] in order to have an idea about the magnitude of these rate coefficients). It should be noted here that reactions (R29) and (R30) do not represent, in fact, loss mechanisms for the $N(^4S)$ atoms with the rate coefficients indicated above, because part of the created N* species may be re-converted again into ground-state atoms. Here, we neglect any reconversion of the N* species into $N(^4S)$ atoms, but this assumption will be analysed in section 4.

As will be shown in section 4, the quenching of $N_2(B\ ^2\Pi_g)$ molecules through reaction (R32) indicated in table 5 plays an important role in the creation of $O(^3P)$ atoms. Here, we use the value proposed in [65], $K_{32} = 3 \times 10^{-10}$ cm^3 s^{-1}, which is in reasonable agreement with the value 2×10^{-10} cm^3 s^{-1} reported in [74]. The analogous reaction with $N_2(A\ ^3\Sigma_u^+)$ has been neglected because the corresponding rate coefficient is two orders of magnitude smaller, 2.54×10^{-12} cm^3 s^{-1} [65].

Finally, the heterogeneous reactions (R9), (R27) and (R33) have been assumed to be first-order processes, that is, with the corresponding rate frequencies related to the probabilities γ by the expression $\nu = \gamma\langle v\rangle/2R$, where $\langle v\rangle$ denotes the average velocity of the particle colliding upon the wall and R is the tube radius. For the wall de-activation process (R9) we use the probability $\gamma = 4.5 \times 10^{-4}$ according to [64] for a pyrex surface, whereas for the re-association of $N(^4S)$ and $O(^3P)$ atoms we use $\gamma = 3.2 \times 10^{-6}$ [71] for the $N(^4S)$ atoms and $\gamma = 5 \times 10^{-3}$ [17] for the case of $O(^3P)$ atoms. The latter value is two times larger than the recent measurement, 2.4×10^{-3}, obtained in [75].

All values reported here for the probabilities γ have been measured in discharges either in pure N_2 or in pure O_2,

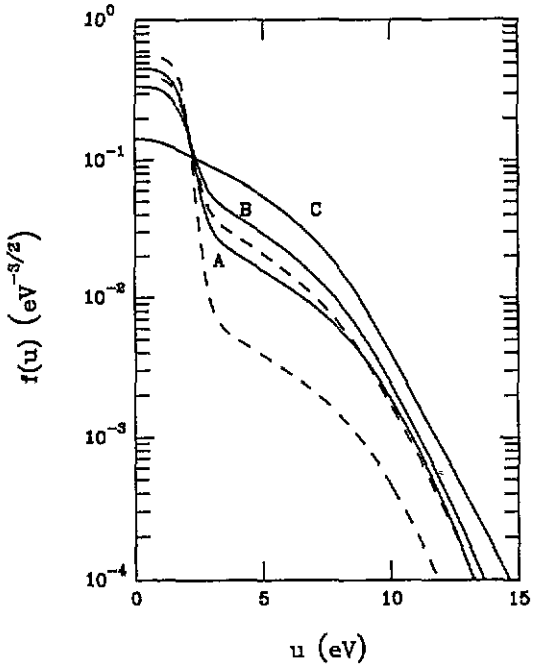

Figure 2. Electron energy distribution functions for $E/p = 15.4$ V cm^{-1} Torr^{-1} and $T_g = 500$ K, in pure N_2 (A), in a 50% N_2–O_2 mixture (B) and in pure O_2 (C). The full curves are for $T_v(N_2) = 4000$ K (A and B) and $T_v(O_2) = 1000$ K (C), whereas the broken ones are for $T_v(N_2) = T_v(O_2) = T_g$. The full and the broken curves are indistinguishable in curve C.

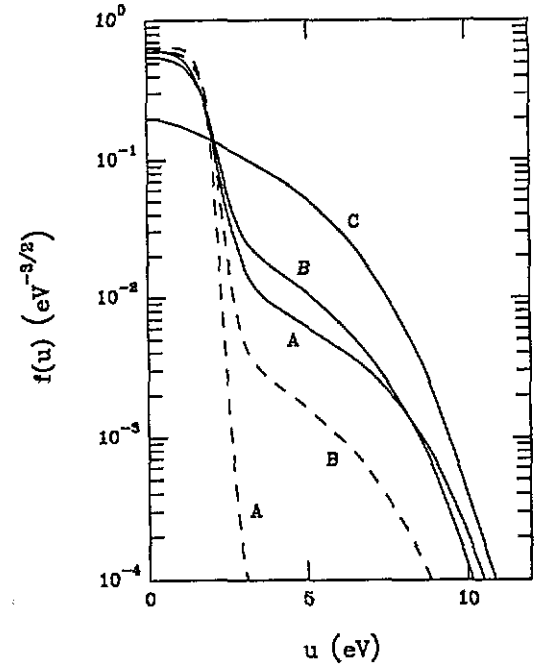

Figure 3. As in figure 2 but for $E/p = 7.73$ V cm^{-1} Torr^{-1}.

because only indirect determinations are known for the case of a N_2–O_2 mixture. For instance, in [6] it was possible to predict the dependences of the probabilities for re-association of N and O atoms on the fractional composition of the mixture δ, from a fitting of calculated concentrations of NO and O to measurements using a kinetic model for surface reactions. We still note that the value 3.2×10^{-6} for the re-association of N(^{4}S) atoms would need to be greatly increased had we considered, as discussed above, the reconversion of N* into N(^{4}S) atoms (see section 4). Finally, a recent determination [76] of the wall probability of reaction (R9) for de-activation of the levels $v = 1$–4 on pyrex has shown our assumption of a constant γ for all vth levels to be realistic.

4. Results and discussion

4.1. Reference model

The calculations in this paper have been carried out for a gas temperature $T_g = 500$ K, which is a typical value found in a low-pressure N_2–O_2 positive column [2, 6]. Moreover, we consider a discharge in a pyrex glass tube of radius $R = 0.8$ cm.

Figure 2 shows the EEDF in a N_2–O_2 mixture calculated for $E/p = 15.4$ V cm^{-1} Torr^{-1} (which corresponds to $E/N = 8 \times 10^{-16}$ V cm^2, p and N denoting the total gas pressure and gas density, respectively), in pure N_2 (curve A), in a mixture with 50% of N_2 (curve B), and in pure O_2 (curve C). The full curves are for the case of significant vibrational excitation of N_2 as characterized by the temperature $T_v(N_2) = 4000$ K, in the case of curves A and B, and for $T_v(O_2) = 1000$ K in curve C, while the broken curves are for $T_v(N_2) = T_v(O_2) = T_g$, that is in the absence of vibrational excitation. The self-consistently determined vibrational temperature of O_2 under the conditions of the full curve B is $T_v(O_2) = 685$ K. This value allows us to conclude that the vibrational temperature of O_2 is close to the gas temperature, as a result of the high V–T rates associated with collisions of $O_2(X, v')$ molecules with O(^{3}P) atoms (reaction (R22) in table 2). Recent measurements of $T_v(O_2)$ under the present discharge conditions in pure O_2 using CARS (coherent anti-Stokes Raman scattering) [77] confirm these predictions. We note that, although the V–T rates in N_2–N and N_2–O collisions are very high, these processes have no marked influence on the lower vth levels of the VDF in N_2, and hence, on the value of $T_v(N_2)$.

The comparison between curves A in figure 2 shows that the presence of vibrationally excited $N_2(X, v)$ molecules gives rise to a strong enhancement of the electron-energy tail of the EEDF, which is a well-known consequence of the effects of the electronic–vibrational (e–V) superelastic collisions [78]. In turn, the EEDFs in pure O_2 for $T_v(O_2) = 1000$ K and $T_v(O_2) = T_g$ are indistinguishable in curve C. Moreover, figure 2 further shows that the EEDFs in pure O_2 have overpopulated electron-energy tails relative to those obtained in pure N_2. This is a consequence of the strong maximum of the electron cross section for vibrational excitation in N_2, at the electron energies of about 2 eV, which causes a sharp decrease in the EEDF at that point.

As is well known in pure N_2 and demonstrated here for a mixture of the type 50% N_2–O_2, the effects caused by the e–V superelastic collisions in N_2 are considerably amplified in the case of lower values of E/p. Figure 3 shows the EEDF calculated for $E/p = 7.73$ V cm^{-1} Torr^{-1}

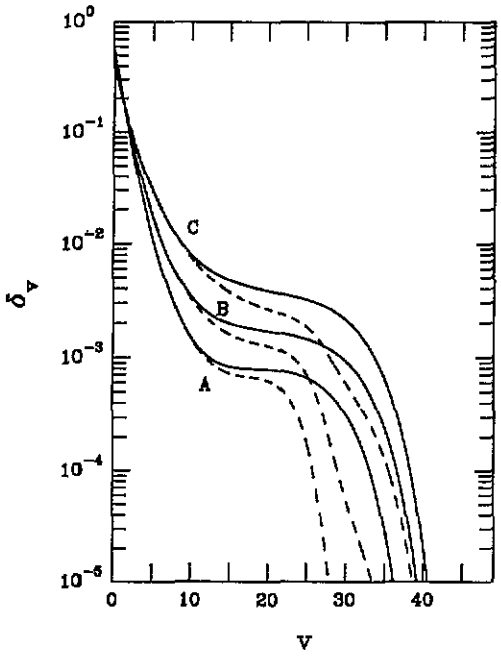

Figure 4. Vibrational distribution functions in N_2 for E/p = 15.4 V cm^{-1} Torr^{-1}, p = 2 Torr, R = 0.8 cm and T_g = 500 K, in pure N_2 (full curves) and in a 90% N_2–O_2 mixture (broken curves), for $T_v(N_2)$ = 3500 (A), 4000 (B) and 5000 K (C).

($E/N = 4 \times 10^{-16}$ V cm^2), keeping all other values as in figure 2. For such a low value of E/p in a 50% N_2–O_2 mixture (curves B), the electrons cannot gain enough energy from the field in order to pass over the barrier formed by the manifold of vibrational levels of N_2. In turn, they can be promoted to the high-energy region due to the effects of the e–V superelastic collisions.

Figure 4 shows the VDFs of $N_2(X, v)$ molecules calculated for E/p = 15.4 V cm^{-1} Torr^{-1} in pure N_2 (full curves) and in a 90% N_2–O_2 mixture (broken curves), for vibrational temperatures $T_v(N_2)$ in the range 3500–5000 K. Here, we have arbitrarily assumed p = 2 Torr ($N = 3.86 \times 10^{16}$ cm^{-3}) according to the measurements in [2, 6]. Furthermore, in order to take into account in our model reactions (R24), (R29) and (R32), we have assumed relative concentrations of $N_2(A\ ^3\Sigma_u^+)$ of $[N_2(A)]/[N_2] = 2 \times 10^{-6}$, 5×10^{-6}, 10^{-5} and 2×10^{-5}, for $T_v(N_2)$ = 3500, 4000, 5000 and 6000 K, respectively, whereas for the $N_2(B\ ^3\Pi_g)$ state we have assumed $[N_2(B)]/[N_2] = 4 \times 10^{-7}$, 10^{-6}, 2×10^{-6} and 4×10^{-6}, for the same values of $T_v(N_2)$. The ratio between the two concentrations was kept constant $[N_2(B)]/[N_2(A)] = 0.2$. All these values are taken from experiments in pure N_2 under the same discharge conditions [79, 80]. We note that the increase in both concentrations is a consequence of the dependence of the temperature $T_v(N_2)$ on the discharge current.

The different curves in figure 4 have been obtained for the temperatures $T_v(N_2)$ = 3500 (A), 4000 (B) and 5000 K (C), which in the case of the broken curves for the 90% N_2–O_2 mixture correspond to the calculated vibrational temperatures of O_2, $T_v(O_2)$ = 810, 905 and 1070 K, respectively. The VDF in pure N_2 has already been analysed in [13]. In that paper it was shown that the characteristic shape of the VDF in N_2 is a result of the combined effects of e–V and V–V exchanges at low vth levels, of near-resonant V–V exchanges at intermediate levels, which lead to the appearance of a plateau in this region, and due to the simultaneous effects of vibrational dissociation propagating down and of V–T exchanges at the higher levels. Now, concerning the VDF of N_2 molecules in a N_2–O_2 mixture, figure 4 shows that relatively low concentrations of O_2, as small as 10%, are large enough to produce a sharp depletion in the VDF. This is a result of the effects of near-resonant V–V exchanges in N_2–O_2 collisions at $v \simeq 28$, of V–T exchanges in N_2–O_2 and N_2–N collisions for $v > 28$ and, to a smaller extent, of V–T N_2–O collisions for $v > 15$ (see figure 1).

Figure 5 shows the VDFs of $O_2(X, v')$ molecules as self-consistently determined by the present model, for E/p = 15.4 V cm^{-1} Torr^{-1}, p = 2 Torr, in the mixtures 90% N_2–O_2 (curves A) and 50% N_2–O_2 (curves B), and for $T_v(N_2)$ = 3500 (full curves), 4000 (broken curves) and 5000 K (dotted curves). We note that the VDFs of O_2 in curves A have been obtained under the same conditions as the VDFs of N_2 plotted as broken curves in figure 4, so they correspond to the temperatures $T_v(O_2)$ = 810, 905 and 1070 K, as $T_v(N_2)$ increases from 3500 up to 5000 K. In turn, the VDFs of O_2 shown in curves B of figure 5 are for $T_v(O_2)$ = 637, 685 and 742 K. Figure 5 shows that, in a N_2–O_2 discharge, the VDFs of O_2 molecules are considerably less excited than those of N_2. This is always true except in the case of a discharge with only slight traces of O_2, in which $T_v(O_2)$ rapidly increases due to the effects of V–V exchanges in N_2–O_2 collisions. We note that, owing to the smaller energy difference in a single-quantum transition in O_2 than in N_2, the most effective V–V reactions between the two molecules correspond to a populating mechanism for O_2 and a depopulating one for N_2. Thus, in the case of the higher temperature $T_v(N_2)$ = 5000 K the vibrational temperature of O_2 molecules increases from 742 K, in the case of a 50% N_2–O_2 mixture, to 1070 K in a 90% N_2–O_2 one, and it reaches the extremely high value $T_v(O_2)$ = 5914 K, that is larger than $T_v(N_2)$, in a mixture with 99% of N_2. However, there is no experimental evidence for this fact and such a high value might be just a consequence of the neglect of the V–T exchanges in O_2-N collisions and of vibrational de-activation of $O_2(X, v')$ on the wall.

Figure 6 shows both vibrational temperatures, for E/p = 15.4 V cm^{-1} Torr^{-1} and p = 2 Torr, as a function of the discharge current $I = \pi R^2 e n_e v_d$, where e is the absolute value of the electron charge, n_e is the electron density assumed constant across the tube and v_d denotes the electron drift velocity. In figure 6 we have plotted both temperatures for the cases of the mixtures 90% N_2–O_2 (full curves) and 50% N_2–O_2 (broken curves). Our predictions indicate that $T_v(N_2)$ increases from 3500 K at I = 2 mA up to 6000 K for I = 40–45 mA, depending on the fractional composition of the mixture. On the other hand, as I increases the temperature $T_v(O_2)$ varies between about 800 K and about 1100 K in a 90% N_2–O_2 mixture, and between about 630 K and about 800 K in the case of a 50% N_2–O_2 mixture.

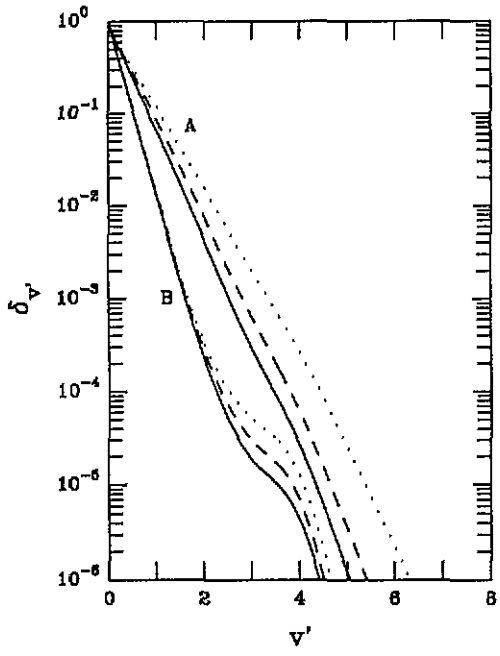

Figure 5. Vibrational distribution functions in O_2 for the same values of E/p, p, R and T_g as in figure 4, calculated in a 90% N_2–O_2 mixture (A) and in a 50% N_2–O_2 mixture (B), for $T_v(N_2) = 3500$ (full curves), 4000 (broken curves) and 5000 K (dotted curves).

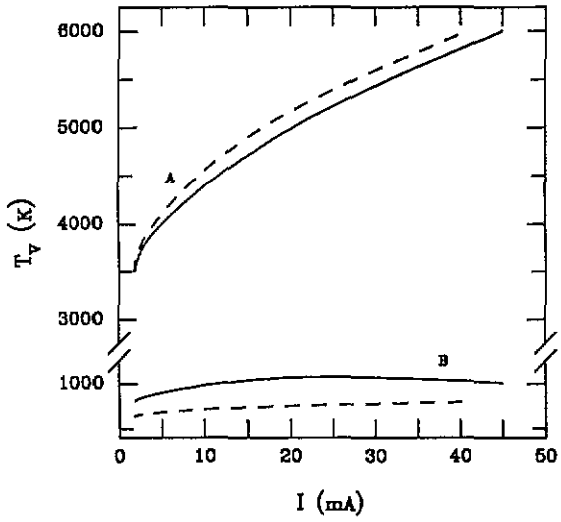

Figure 6. Vibrational temperatures $T_v(N_2)$ (A) and $T_v(O_2)$ (B), as a function of the discharge current, calculated in a 90% N_2–O_2 mixture (full curves) and in a 50% N_2–O_2 mixture (broken curves), for the same values of E/p, p, R and T_g as in figures 4 and 5.

Figures 7-9 show, as a function of the relative concentration of total oxygen in the mixture $1-[N_2]/N \simeq [O_2]/N + [O]/N$ (the concentrations of N and NO are always less than 0.5% and 2%, respectively) the relative concentrations of NO($X\ ^2\Pi_r$) molecules and N(^{4}S) and O(^{3}P) atoms. As before, the results have been obtained for $E/p = 15.4$ V cm^{-1} Torr^{-1}, $p = 2$ Torr and $T_v(N_2) = 3500$ (full curves), 5000 (broken curves) and 6000 K (dotted curves). The global behaviour exhibited by these concentrations is in qualitative agreement with the measurements reported in [2, 6]. These measurements

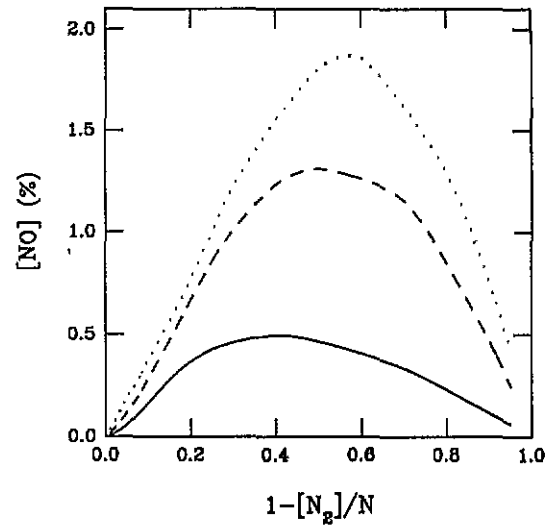

Figure 7. The relative concentration of NO($X\ ^2\Pi_r$) molecules as a function of the concentration of total oxygen (molecular plus atomic oxygen) in a N_2–O_2 mixture, for $E/p = 15.4$ V cm^{-1} Torr^{-1}, $p = 2$ Torr, $R = 0.8$ cm, $T_g = 500$ K, for $T_v(N_2) = 3500$ (full curve), 5000 (broken curve) and 6000 K (dotted curve).

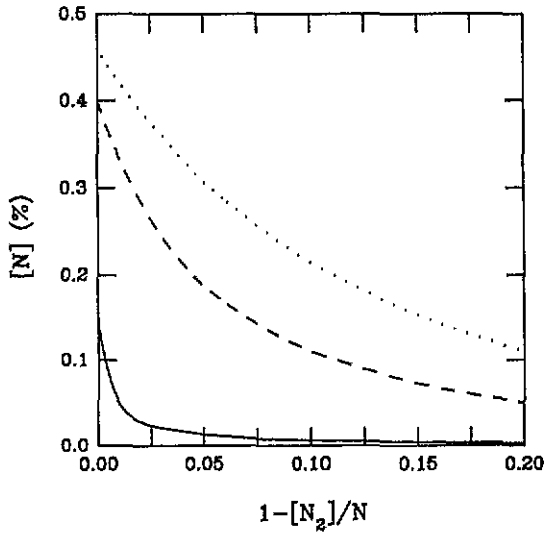

Figure 8. The relative concentration of N(^{4}S) atoms under the same conditions as in figure 7.

have not been plotted because we are not seeking here a fit of theory to experiment. In particular, we do not fit the probabilities for the reactions on the wall but are just using data from the literature for the pure gases.

As a result of the linked kinetics, figures 7 and 9 show that the [NO] and [O] concentrations pass through a maximum for N_2–O_2 mixtures with approximately equal proportions of the two gases. On the other hand, figure 8 shows that a very small concentration of O_2 is large enough to produce a rapid decrease in the concentration of N(^{4}S) atoms. The decrease in [N] concentration is a consequence of the extremely high loss rate of reaction (R16) for the quenching of N(^{4}S) atoms by NO molecules. It should be remembered here that in a discharge in pure N_2, the most important mechanisms for dissociation occur via electron impact or through the V–V and V–T energy exchange

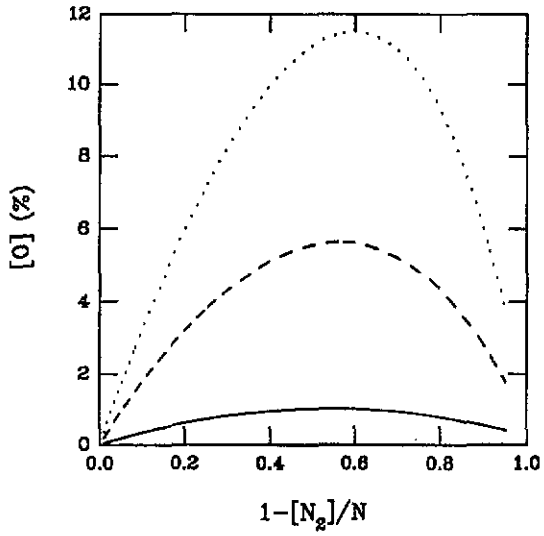

Figure 9. The relative concentration of $O(^3P)$ atoms under the same conditions as in figure 7.

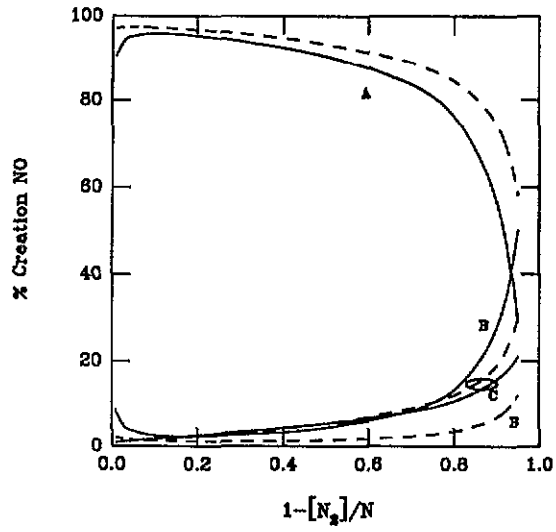

Figure 10. Percentage contributions of the various creation processes of $NO(X\ ^2\Pi_r)$ molecules for $T_v(N_2) = 3500$ (full curves) and 5000 K (broken curves), under the same conditions as in figure 7: curves A, reaction (R15); curves B, reaction (R23); and curves C, reaction (R24).

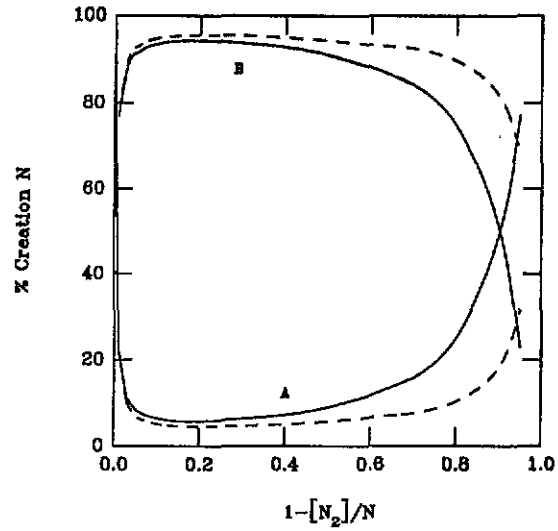

Figure 11. Percentage contributions of the various creation processes of $N(^4S)$ atoms for $T_v(N_2) = 3500$ (full curves) and 5000 K (broken curves), under the same conditions as in figure 8: curves A, electron impact; curves B, reaction (R15).

processes, the latter being predominant at low E/p [13, 14]. However, under the conditions of figure 8, in pure N_2, the value of E/p is not small enough for the rate of dissociation by V–V and V–T processes to become significant, in part due to the strong de-activation exerted upon the VDF by the V–T exchanges in N_2–N collisions. Note that, although $T_v(N_2)$ is fixed in figures 7–9, the discharge current is not kept constant as $\delta(N_2)$ varies. In fact, as $1 - [N_2]/N$ increases from 0 to 0.95, we obtain decreasing values $I = 1.8$–1.2 mA for $T_v(N_2) = 3500$ K, $I = 20.0$–4.9 mA for 5000 K and $I = 43.5$–11.1 mA for 6000 K.

In figures 10–12 we present the percentage contributions of the various processes to the total production of NO, N and O, as a function of the total oxygen concentration in the mixture (molecular plus atomic oxygen), under the same conditions as in figures 7–9 except that here we only plot curves for $T_v(N_2) = 3500$ K and 5000 K.

Figure 10 shows that the most important mechanism for creation of NO molecules is through reaction (R15), involving the collision of O atoms with the vibrationally excited $N_2(X, v)$ molecules in levels $v \geq 13$. Other non-negligible mechanisms are reactions (R23) and (R24) in table 3, but both may become important only in mixtures predominantly constituted by O_2. The effects of the three-body reaction (R25) are always negligibly small. Therefore, the present study shows that the [NO] concentration is only slightly affected by the assumed populations of the metastable molecule $N_2(A\ ^3\Sigma_u^+)$. Reaction (R16) constitutes practically the only mechanism present for NO losses, except in the limit of the higher O_2 concentrations, at which the destruction via the three-body reaction (R26) may become important (about 25% of the total loss rate in the case of a 5% N_2–O_2 mixture).

Figure 11 shows that reaction (R15) is also the major mechanism for the production of $N(^4S)$ atoms in a N_2–O_2 mixture. Dissociation by electron impact (R10) constitutes the major mechanism in pure N_2 (or in the opposite case of a mixture with traces of N_2 only, as a result of the increase in the high-energy tail of the EEDF and of a small presence of NO). In a mixture with a very small fraction of O_2, reaction (R15) rapidly becomes predominant (about 77% of the total rate in a 99% N_2–O_2 mixture). The dissociation by the V–V and V–T processes (R11)–(R13) is always negligibly small due to the de-activation of the VDF either by V–T processes in N_2–N collisions or by reaction (R15). The $N(^4S)$ atoms are mainly destroyed by collisions with the metastable species $N_2(A\ ^3\Sigma_u^+)$ or by electron impact (reactions (R29) and (R30)) in pure N_2 (see further discussion in figure 18 later), and through collisions with NO molecules (via reaction (R16)) in the case of a N_2–O_2 mixture. The contribution of reaction (R16) to the total loss rate of $N(^4S)$ atoms is about 80% in a 99% N_2–O_2 mixture and increases to 98% for higher concentrations of

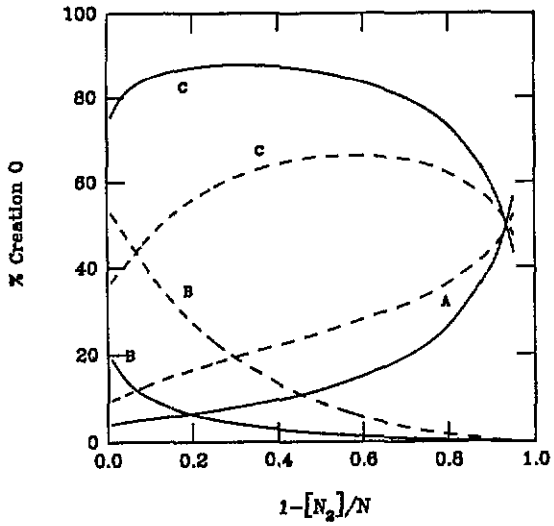

Figure 12. Percentage contributions of the various creation processes of $O(^3P)$ atoms for $T_v(N_2) = 3500$ (full curves) and 5000 K (broken curves), in the same conditions as in figure 9: curves A, electron impact; curves B, reaction (R16); and curves C, reaction (R32).

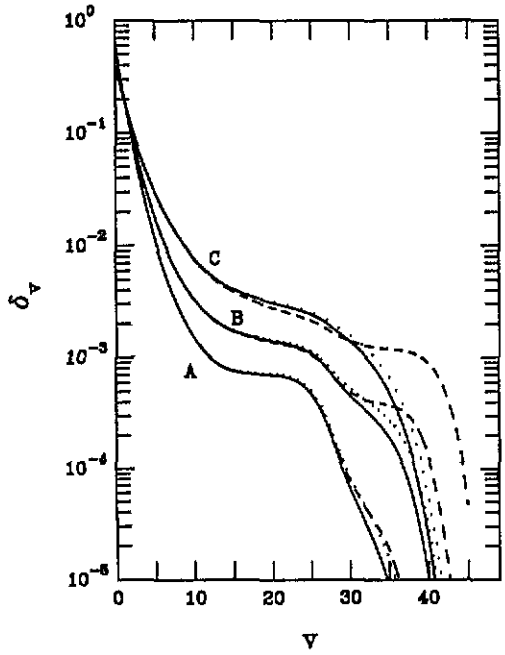

Figure 13. Vibrational distribution functions in N_2 in a 95% N_2–O_2 mixture, for $E/p = 15.4$ V cm^{-1} Torr^{-1}, $p = 2$ Torr, $R = 0.8$ cm, $T_g = 500$, for $T_v(N_2) = 3500$ (A), 4000 (B) and 5000 K (C). The full curves are for our base model, whereas the broken and the dotted curves are obtained in the absence of V–T N_2–N and of V–T N_2–O collisions, respectively.

O_2. Therefore, the populations of NO and N are strongly correlated.

Figure 12 shows that the collisions of the excited $N_2(B\ ^3\Pi_g)$ molecules with O_2 (reaction (R32)) are the most important mechanism for creation of atomic oxygen $O(^3P)$. However, since in this paper the concentrations of the electronic $N_2(B\ ^3\Pi_g)$ state have been assumed, figures 9 and 12 are merely indicative. The $O(^3P)$ atoms are also created via reaction (R16) in mixtures

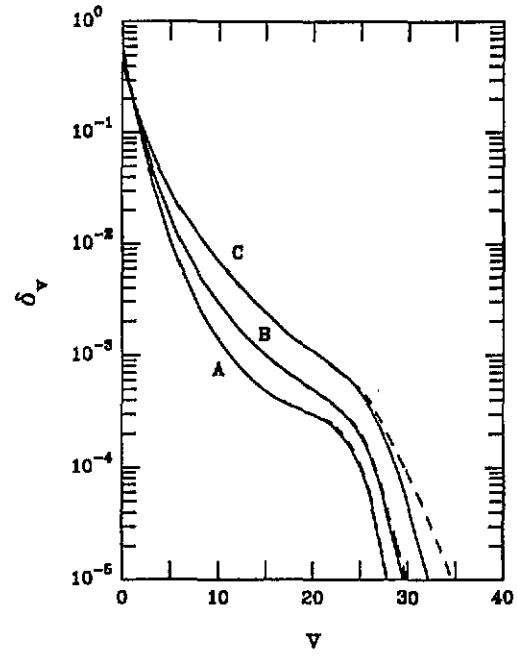

Figure 14. As in figure 13 but for $K_{15}^v = 10^{-12}$ cm^3 s^{-1} (see text), in the case of our base model (full curves) and in the absence of V–T N_2–N collisions (broken curves).

predominantly formed by N_2, or by electron impact in mixtures predominantly constituted by O_2. We note that the conclusions extracted from figure 12 are probably affected by the fact that the values of I decrease as $1 - [N_2]/N$ increases. An increasing importance of the dissociation by electron impact would have been found had we kept the discharge current constant in figure 12. The major loss mechanism for $O(^3P)$ atoms is re-association on the wall.

4.2. Omitting or changing some processes

As we have pointed out before, the kinetics of the species under analysis are strongly correlated through the VDF of N_2 molecules which is highly dependent on the magnitude of the rate coefficients for the various V–T processes. In particular, the final shape exhibited by the VDF is highly dependent on the V–T rates for N_2–N collisions (reactions (R6) and (R7)) and N_2–O collisions (reaction (R8)) and on the rate coefficient of reaction (R15). Unfortunately, all these rates are subject to large uncertainties.

In order to evaluate the above dependences, we present in figure 13 the VDF of N_2 molecules for the same values of E/p and $T_v(N_2)$ as in figure 4, in the case of a 95% N_2–O_2 mixture, calculated now in the absence of either V–T N_2–N or V–T N_2–O collisions. For comparison we also plot in figure 13 the VDF obtained from our reference model. Figure 13 shows that, in the absence of V–T processes in N_2–N collisions, the VDF significantly increases for the levels $v > 28$. On the other hand, if we discard the V–T processes associated with N_2–O collisions, then the increase in the VDF occurs, but to a smaller extent, at lower vth levels. This behaviour is a consequence of the dependences of the rates for both processes on the vth quantum number. In figure 1 we have shown that the V–T rates in N_2–N collisions rapidly increase with the vth quantum number

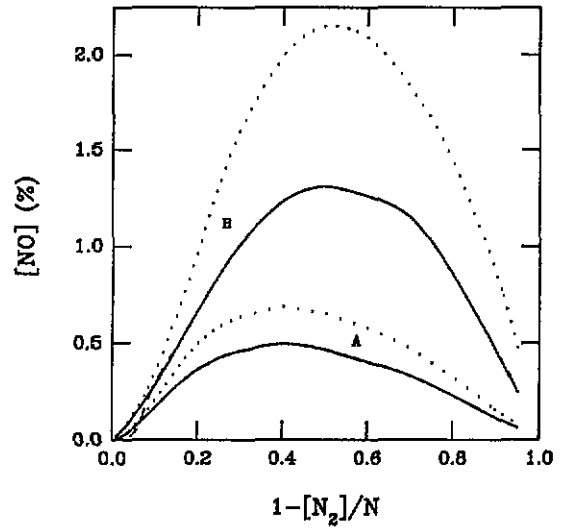

Figure 15. The relative concentration of NO($X\ ^2\Pi_r$) molecules as a function of the total oxygen concentration in a N_2–O_2 mixture, for $E/p = 15.4$ V cm^{-1} Torr^{-1}, $p = 2$ Torr, $R = 0.8$ cm, $T_g = 500$ K, for $T_v(N_2) = 3500$ (A) and 5000 K (B). The full curves are for our base model, whereas the broken and the dotted curves are obtained in the absence of V–T N_2–N and of V–T N_2–O collisions, respectively. The broken curves are indistinguishable from the full ones except near the origin of the axes.

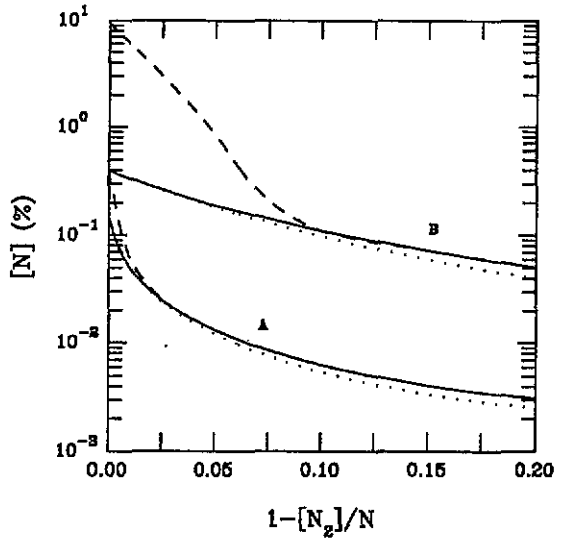

Figure 16. As in figure 15 but here for the concentration of N(^{4}S) atoms.

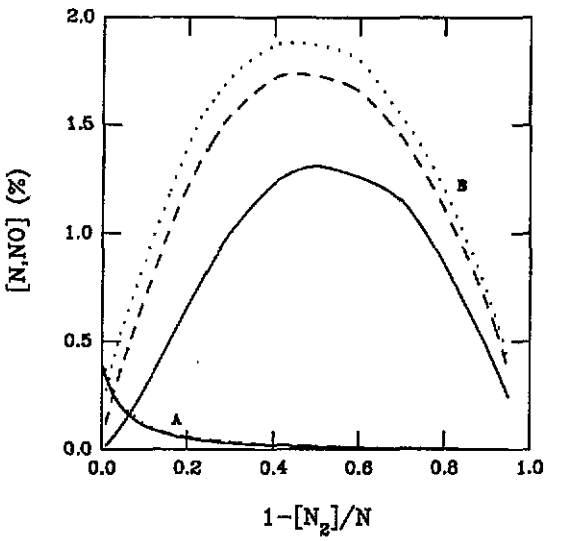

Figure 17. The relative concentration of N(^{4}S) atoms (curves A) and NO($X\ ^2\Pi_r$) molecules (curves B), for $E/p = 15.4$ V cm^{-1} Torr^{-1}, $p = 2$ Torr, for $T_v(N_2) = 5000$ K, as the rate coefficient of reaction (R15) increases from 10^{-13} cm^3 s^{-1} (full curves), to 10^{-12} cm^3 s^{-1} (broken curves) and to 10^{-11} cm^3 s^{-1} (dotted curves). The curves A are practically indistinguishable.

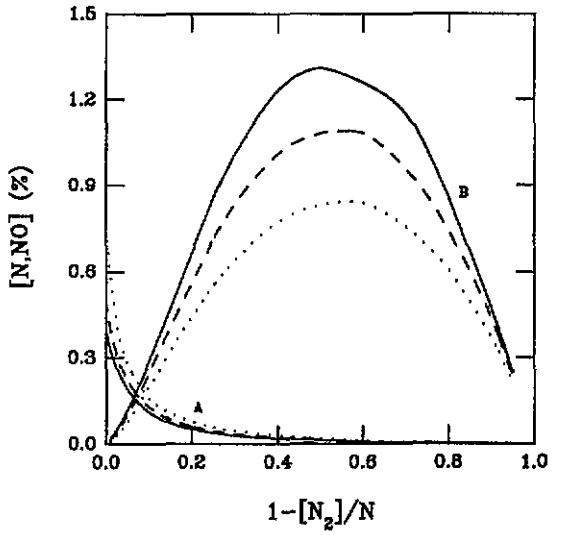

Figure 18. The relative concentration of N(^{4}S) atoms (curves A) and NO($X\ ^2\Pi_r$) molecules (curves B), for $E/p = 15.4$ V cm^{-1} Torr^{-1}, $p = 2$ Torr, for $T_v(N_2) = 5000$ K, assuming the following percentage for the re-conversion of N(^{2}D, ^{2}P) atoms into N(^{4}S) (see text): 0% (full curves); 20% (broken curves); and 50% (dotted curves).

by seven orders of magnitude, presenting for $v > 28$ the highest rates among those for the various V–T processes. In contrast, the dependence of the V–T N_2–O rates on the vth level is much flatter so this mechanism plays a major role at the lower vth levels.

The effects of both V–T rates are progressively smaller either as the percentage of O_2 increases or as a higher value for the rate coefficient of reaction (R15) is assumed. Figure 14 shows the VDF obtained under the same conditions as in figure 13 but assuming $K_{15}^v = 10^{-12}$ cm^3 s^{-1} for $v \geq 13$ in reaction (R15). We note that a still higher value, 10^{-11} cm^3 s^{-1}, has been estimated in [6] from a fit to the relative variation of the N_2^+(B) 391.4 nm band in a N_2–O_2 glow discharge. As stated in that paper, the N_2^+(B) state seems to be mainly produced by the reaction $N_2(X, v > 12) + N_2^+(X) \rightarrow N_2(X, v-12) + N_2^+(B)$, which involves the de-excitation of the VDF. However, in [6] the V–T exchanges in N_2–N collisions were not taken into account, so that a larger rate coefficient for reaction (R15) was needed in that paper in order to obtain an equivalent depopulation of the $N_2(X, v)$ molecules.

Figures 15 and 16 show the relative concentrations of NO molecules and of N(^{4}S) atoms when the V–T N_2–N or the V–T N_2–O processes are discarded (in the case of our reference model with $K_{15}^v = 10^{-13}$ cm^3 s^{-1}). Figure 15

shows that, for the present choice of K_{15}^{v}, the effects on the [NO] concentration of the V–T rates in N_2–N collisions are vanishingly small, whereas those corresponding to N_2–O collisions may be extremely important. We note that the NO molecules, being created through reaction (R15), are strongly dependent on the populations in $N_2(X, v)$ levels just above $v \geq 13$. In contrast, figure 16 shows that the concentration of $N(^4S)$ atoms is mainly dependent on the V–T exchanges involving the N atoms themselves. In the absence of V–T N_2–N collisions, in a mixture with a small percentage of O_2, the VDF of N_2 rapidly increases at the higher vth levels, producing the appearance of dissociation by the V–V and V–T mechanisms. This effect occurs predominantly in pure N_2, where it is independent of the magnitude of the rate coefficient K_{15}^{v}. The concentration of $N(^4S)$ atoms is only slightly modified by the neglect of V–T N_2–O collisions. Neither V–T process under analysis plays a significant role in determining the concentration of $O(^3P)$ atoms, since the latter is mainly determined by dissociation by electron impact and by reaction (R32) involving the collisions of $N_2(B\ ^3\Pi_g)$ molecules with O_2.

In order to evaluate the direct effects of the large uncertainties in the rate coefficient of reaction (R15) upon the relative concentrations of NO molecules and N atoms, figure 17 shows both concentrations calculated for $E/p = 15.4$ V cm^{-1} Torr^{-1}, $p = 2$ Torr and $T_v(N_2) = 5000$ K, considering the values 10^{-13}, 10^{-12} and 10^{-11} cm^3 s^{-1} for this rate coefficient. Owing to a very strong coupling with the VDF of N_2 molecules, the increase by two orders of magnitude in K_{15}^{v}, from 10^{-13} to 10^{-11} cm^3 s^{-1}, produces a completely negligible modification in [N] and only a relatively small increase in [NO]. In the case of a 50% N_2–O_2 mixture the relative concentration of NO increases from 1.31% to 1.87% as K_{15}^{v} increases by two orders of magnitude.

One point of inconsistency in our model is the neglect of the kinetics of the atomic metastable species $N(^2D)$ and $N(^2P)$, although it is known that these species are formed by the reactions (R24), (R29) and (R30). Here, we have assumed that the excited atoms re-combine into $N_2(X, v = 0)$ molecules through reaction (R14), so we neglect any re-conversion of these species into $N(^4S)$ atoms. In order to evaluate this assumption, we present in figure 18 the concentrations of $N(^4S)$ atoms and NO molecules, under the same conditions as in figure 17 with $K_{15}^{v} = 10^{-13}$ cm^3 s^{-1}, but assuming that 20% and 50% of $N(^2D, ^2P)$ atoms are re-converted into $N(^4S)$ (plotted as broken and dotted curves, respectively). Figure 18 shows that the concentration of NO is overestimated by the present model, while that of N atoms is somewhat underestimated. We note that the probability for wall re-association of $N(^4S)$ atoms, which in the present paper is assumed constant and equal to 3.2×10^{-6}, would have to be greatly increased to obtain the same $N(^4S)$ concentration if the processes (R29) and (R30) for destruction of $N(^4S)$ atoms were discarded (that is, in the case of a complete re-conversion of $N(^2D, ^2P)$ atoms). For instance, under the conditions of figure 18 in pure N_2, γ should take the value 7×10^{-4} in order to obtain the same concentration of $N(^4S)$ atoms as before. Future work should take into account the kinetics of both atomic metastable species in a fully self-consistent way.

5. Conclusions

In this paper we carried out a kinetic study of a low-pressure stationary discharge in a N_2–O_2 mixture. This study focused on the role played by the distribution of the vibrationally excited molecules $N_2(X\ ^1\Sigma_g^+, v > 0)$ on the overall kinetics, in particular, on the concentrations of the ground-state $NO(X\ ^2\Pi_r)$ molecule and of $N(^4S)$ and $O(^3P)$ atoms. The various mechanisms for production and loss of each of these species were analysed in detail, as was the coupling among the corresponding kinetics and to the distribution of $N_2(X, v)$ molecules. Although the predicted concentrations are in fair agreement with the measurements, we have not attempted here to fit to experiment in order to derive unknown data for a number of elementary processes. The probabilities for the different heterogeneous reactions on the wall were also considered constant, with values as given in the literature.

Our results show that the populations of NO molecules and N atoms are strongly correlated, since both of them are mainly created and destroyed through the same two reactions, $N_2(X, v \geq 13) + O \rightarrow NO + N$ and $NO + N \rightarrow N_2(X, v \simeq 3) + O$. Thus, these populations are principally determined by other mechanisms and the rate coefficients for these processes cannot be estimated by a fitting to the populations of NO and N. Furthermore, an accurate prediction of the distribution of $N_2(X, v)$ molecules is of capital importance in the kinetics as a whole, which is in part due to the fact that only vibrationally excited molecules in levels $v \geq 13$ may produce NO and N.

On the other hand, the distribution of $N_2(X, v)$ molecules may be strongly de-activated by the joint action of the two above-mentioned reactions and by the vibrational–translational (V–T) energy exchange processes. Therefore, two limiting situations can occur, in principle. (i) In the case of a rate coefficient for the reaction $N_2(X, v \geq 13) + O \rightarrow NO + N$ not larger than 10^{-13} cm^3 s^{-1}, the vibrational distribution is mainly de-excited by V–T processes. (ii) In the opposite case, that is, for higher values of the rate coefficient of this reaction, the $N_2(X, v)$ molecules are efficiently destroyed by this mechanism.

In spite of the complexity of these kinetics, in previous work it was possible to obtain very good agreement between theory and experiment by an appropriate choice of the rate coefficient for the reaction $N_2(X, v \geq 13) + O \rightarrow NO + N$ and the probabilities for wall losses of N and O atoms under mixture conditions [6]. However, in that work the V–T exchanges in N_2–N collisions were neglected so that the rate coefficient of the above reaction, leading to formation of NO and N, may be somewhat overestimated. In [6] the value 10^{-11} cm^3 s^{-1} was found, whereas the average value from the literature is 10^{-13} cm^3 s^{-1}. Although we have followed a different approach here the main conclusions of the present paper are, in their general trends, in agreement with the conclusions of that previous work.

Nevertheless, this paper presents some weaknesses which should be pointed out. First of all, the model assumes a constant electric field which makes it difficult to compare theory to experiment. Usually, it is the pressure and the

discharge current which are kept constant in an experiment and not the electric field. The sustaining electric field necessary for the steady-state operation of the discharge is obtained, as is well known, from the balance between the total rate of ionization, including step-wise ionization by electron impact and associative ionization, and the total rate of electron loss. The determination of the discharge characteristics was outside the scope of this work, but future work should concentrate on this point.

Secondly, the model should include the kinetics of the excited electronic states $N_2(A\,^3\Sigma_u^+)$ and $N_2(B\,^3\Pi_g)$, whose concentrations were estimated from discharges in pure N_2 and were given in this paper as inputs, as well as those of other states playing an important role in associative ionization such as $N_2(a'\,^1\Sigma_u^-)$ and $N_2(a''\,^1\Sigma_g^+)$ [81–83]. Finally, the work should be extended in order to include the kinetics of the metastable atomic states $N(^2D)$ and $N(^2P)$.

In conclusion, future work should mainly concentrate on the above points in order to improve the accuracy of the description. However, the present model is satisfactory on physical ground since it provides an insight into the basic kinetic processes occurring in these discharges.

Acknowledgments

The authors would like to thank Professor C M Ferreira and Dr B Gordiets for many fruitful discussions and valuable suggestions. We also would like to acknowledge the collaboration of Drs M Touzeau, D Pagnon, J Nahorny and M Vialle in this work.

References

[1] Gordiets B and Ricard A 1993 *Plasma Sources Sci. Technol.* **2** 158
[2] Nahorny J, Pagnon D, Touzeau M, Vialle M, Gordiets B and Ferreira C M 1995 *J. Phys. D: Appl. Phys.* **28** 738
[3] De Souza A R, Mahlmann C M, Muzart J L and Speller C V 1993 *J. Phys. D: Appl. Phys.* **26** 2164
[4] Granier A 1993 *Microwave Discharges: Fundamentals and Applications* ed C M Ferreira and M Moisan (New York: Plenum) pp 491–501
[5] Granier A, Chéreau D, Henda K, Safari R and Leprince P 1994 *J. Appl. Phys.* **75** 104
[6] Gordiets B, Ferreira C M, Guerra V, Loureiro J, Nahorny J, Pagnon D, Touzeau M and Vialle M 1995 *IEEE Trans. Plasma Sci.* to be published
[7] Premachandran V 1989 *Appl. Phys. Lett.* **55** 2488
[8] Lin T H, Belser M and Tzeng Y 1988 *IEEE Trans. Plasma Sci.* **16** 631
[9] Yasuda Y, Zaima S, Kaida T and Koide Y 1990 *J. Appl. Phys.* **67** 2603
[10] Rusanov V D and Fridman A A 1976 *Sov. Phys. – Dokl.* **21** 739
[11] Macheret S O, Rusanov V L, Fridman A A and Sholin G V 1980 *Sov. Phys. – Tech. Phys.* **25** 421
[12] Kochetov I V, Mishin E V and Telegin V A 1986 *Sov. Phys. – Dokl.* **31** 990
[13] Loureiro J and Ferreira C M 1986 *J. Phys. D: Appl. Phys.* **19** 17
[14] Loureiro J 1991 *Chem. Phys.* **157** 157
[15] Rohlena K and Masek K 1985 *Acta Phys. Slovaca* **35** 141
[16] Ferreira C M and Loureiro J 1989 *J. Phys. D: Appl. Phys.* **22** 76
[17] Gousset G, Touzeau M, Vialle M and Ferreira C M 1989 *Plasma Chem. Plasma Process.* **9** 189
[18] Gousset G, Ferreira C M, Pinheiro M, Sá P A, Touzeau M, Vialle M and Loureiro J 1991 *J. Phys. D: Appl. Phys.* **24** 290
[19] Láska L, Masek K and Ruzicka T 1979 *Czech. J. Phys.* B **29** 498
[20] Pinheiro M 1993 *PhD Thesis* Universidade Técnica de Lisboa
[21] Frost L S and Phelps A V 1962 *Phys. Rev.* **127** 1621
[22] Loureiro J and Ricard A 1993 *J. Phys. D: Appl. Phys.* **26** 163
[23] Lofthus A and Krupenie P H 1977 *J. Phys. Chem. Ref. Data* **6** 113
[24] Krupenie P H 1972 *J. Phys. Chem. Ref. Data* **1** 423
[25] Stogryn D E and Stogryn A P 1966 *Mol. Phys.* **11** 371
[26] Schulz G J 1973 *Rev. Mod. Phys.* **45** 423
[27] Laganà A, Garcia E and Ciccarelli L 1987 *J. Phys. Chem.* **91** 312
[28] Armenise I, Capitelli M, Garcia E, Gorse C, Laganà A and Longo S 1992 *Chem. Phys. Lett.* **200** 597
[29] Frost R J and Smith I W M 1987 *Chem. Phys. Lett.* **140** 499
[30] Cacciatore M, Capitelli M and Gorse C 1982 *Chem. Phys.* **66** 141
[31] Geltman S 1973 *J. Quant. Spectrosc. Radiat. Transfer* **13** 601
[32] Berrington K A, Burke P G and Robb W D 1975 *J. Phys. B: At. Mol. Phys.* **8** 2500
[33] Loureiro J and Ferreira C M 1989 *J. Phys. D: Appl. Phys.* **22** 67
[34] Zipf E C and McLaughlin R W 1978 *Planet. Space Sci.* **26** 449
[35] Winters H F 1966 *J. Chem. Phys.* **44** 1472
[36] Schwartz R N, Slawsky Z I and Herzfeld K F 1952 *J. Chem. Phys.* **20** 1591
[37] Schwartz R N and Herzfeld K F 1954 *J. Chem. Phys.* **22** 767
[38] Keck J and Carrier G 1965 *J. Chem. Phys.* **43** 2284
[39] Bray K N C 1968 *J. Phys. B: At. Mol. Phys.* **1** 705
[40] Billing G D and Fisher E R 1979 *Chem. Phys.* **43** 395
[41] Capitelli M, Gorse C and Billing G D 1980 *Chem. Phys.* **52** 299
[42] Bogdanov A V, Dubrovskii G V, Gorbachev Yu E and Strelchenya V M 1989 *Phys. Rep.* **181** 121
[43] Kunc J A 1991 *J. Phys. B: At. Mol. Opt. Phys.* **24** 3741
[44] Gilmore F R, Bauer E and McGowan J W 1969 *J. Quant. Spectrosc. Radiat. Transfer* **9** 157
[45] Billing G D and Jolicard G 1982 *Chem. Phys.* **65** 323
[46] Billing G D and Kolesnick R E 1992 *Chem. Phys. Lett.* **200** 382
[47] Huber K P and Herzberg G 1979 *Molecular Spectra and Molecular Structure: Constants of Diatomic Molecules* (New York: Van Nostrand Reinhold)
[48] Billing G D 1994 *Chem. Phys.* **179** 463
[49] Eckstrom D J 1973 *J. Chem. Phys.* **59** 2787
[50] McNeal R J, Whitson Jr M E and Cook G R 1974 *J. Geophys. Res.* **79** 1527
[51] Kiefer J H 1972 *J. Chem. Phys.* **57** 1938
[52] Lutz R W and Kiefer J H 1966 *Phys. Fluids* **9** 1638
[53] Millikan R C and White D R 1963 *J. Chem. Phys.* **39** 98
[54] Parker J C 1964 *J. Chem. Phys.* **41** 1600
[55] Eliasson B and Kogelschatz U 1986 Brown Boveri report KLR 86-11 C
[56] Breen J E, Quy R B and Glass G P 1973 *J. Chem. Phys.* **59** 556
[57] Kiefer J H and Lutz R W 1967 *11th Symp. Combustion, Berkeley, CA (1966)* p 67
[58] Breig E L 1969 *J. Chem. Phys.* **51** 4539
[59] Webster III H and Bair E J 1972 *J. Chem. Phys.* **56** 6104
[60] Gordiets B F 1977 *Geomagn. Aeronomia* **17** 871 (in Russian)

[61] Rusanov V D and Fridman A A 1984 *Physics of Chemically Active Plasma* (Moscow: Nauka) (in Russian)
[62] Polak L S, Goldenberg M Ya and Levitski A A 1984 *Numerical Methods in Chemical Kinetics* (Moscow: Nauka) (in Russian)
[63] Dmitrieva I K and Zenevich V A 1984 *Khim. Fiz.* **3** 1075 (in Russian)
[64] Black G, Sharpless R L and Slanger T G 1973 *J. Chem. Phys.* **58** 4792
[65] Kossyi I A, Kostinsky A Yu, Matveyev A A and Silakov V P 1992 *Plasma Sources Sci. Technol.* **1** 207
[66] Baulch D L, Cox R A, Hampson Jr R F, Kerr J A, Troe J and Watson R T 1980 *J. Phys. Chem. Ref. Data* **9** 295
[67] Winkler I C, Stachnik R A, Steinfeld J I and Miller S M 1986 *J. Chem. Phys.* **85** 890
[68] Gilibert M, Aguilar A, Gonzalez M and Sayss R 1993 *Chem. Phys.* **172** 99
[69] Piper L G, Caledonia G E and Kennealy J P 1981 *J. Chem. Phys.* **75** 2847
[70] Piper L G 1982 *J. Chem. Phys.* **77** 2373
[71] Yamashita T 1979 *J. Chem. Phys.* **70** 4248
[72] Piper L G 1989 *J. Chem. Phys.* **90** 7087
[73] Young R A and St John G A 1968 *J. Chem. Phys.* **48** 895
[74] Piper L G 1992 *J. Chem. Phys.* **97** 270
[75] Magne L, Coitout H, Cernogora G and Gousset G 1993 *J. Physique. III* **3** 1871
[76] Parish J W and Yaney P P 1994 *Proc. 47th Annual Gaseous Electronics Conf., Gaithersburg, MA Bull. Am. Phys. Soc.* **39** 1473
[77] Lefebvre M, Pealat M, Gousset G, Touzeau M and Vialle M 1990 *Proc. X ESCAMPIG, Orléans* vol 14E, ed B Dubreuil and K Bethge Europhysics Conference Abstracts pp 246–7
[78] Nighan W L 1970 *Phys. Rev.* A **2** 1989
[79] Cernogora G, Ferreira C M, Hochard L, Touzeau M and Loureiro J 1984 *J. Phys. B: At. Mol. Phys.* **17** 4429
[80] Ferreira C M, Touzeau M, Hochard L and Cernogora G 1984 *J. Phys. B: At. Mol. Phys.* **17** 4439
[81] Polak L S, Sergeev P A and Slovetskii D I 1977 *High Temp.* **15** 13
[82] Golubovskii Yu B and Telezhko V M 1984 *High Temp.* **22** 340
[83] Brunet H and Serra J R 1985 *J. Appl. Phys.* **57** 1574